High Curie Temperature Bismuth-Based Piezo-/Ferroelectric Single Crystals of Complex Perovskite Structure: Recent Progress and Perspectives

Journal:	*CrystEngComm*
Manuscript ID	CE-HIG-07-2021-000962.R1
Article Type:	Highlight
Date Submitted by the Author:	24-Sep-2021
Complete List of Authors:	Liu, Zenghui; Xi'an Jiaotong University, ; Simon Fraser University , Department of Chemistry Wu, Hua; Donghua University, Applied Physics Zhuang, Jian; Xi'an Jiaotong University, Niu, Gang; Xi'an Jiaotong University, Electronic Sci.&Technol. Zhang, Nan; Xi'an Jiaotong University, a. Electronic Materials Research Laboratory, Key Laboratory of the Ministry of Education & International Center for Dielectric Research Ren, Wei; Xi'an Jiaotong University, Ye, Zuo-Guang; Simon Fraser University, Chemistry

SCHOLARONE™
Manuscripts

HIGHLIGHT

High Curie Temperature Bismuth-Based Piezo-/Ferroelectric Single Crystals of Complex Perovskite Structure: Recent Progress and Perspectives

Zenghui Liu*[a], Hua Wu[b], Jian Zhuang[a], Gang Niu*[a], Nan Zhang[a], Wei Ren[a] and Zuo-Guang Ye*[c]

Piezo-/ferroelectrics are essential materials for electromechanical sensors and actuators and energy harvesters in a wide range of technological applications. The demand for piezo-/ferroelectric materials with high Curie temperature (T_C) arises from numerous emerging applications such as downhole oil and gas explorations, automobiles, petrochemistry, metallurgy, and nuclear energy and aerospace industries, in which the electromechanical devices have to operate at elevated temperatures. However, it is a long-standing challenge to simultaneously obtain high piezoelectricity and high T_C. Recently, significant progress has been made on bismuth-based piezo-/ferroelectric single crystals (BPSCs) which show excellent piezoelectric performance and high T_C, proving to be a promising family of novel materials for high-temperature electromechanical applications. In this highlight, we review the recent progress in BPSCs with focus on materials design, crystal growth, physical properties, crystal chemistry, and complex domain structures. In addition, the future perspectives of BPSCs are discussed.

1. Introduction

Piezo-/ferroelectric materials can generate electric signals when environmental mechanical forces are applied, and vice versa, produce mechanical responses under electric fields. Therefore, they are widely used as electromechanical transducers (sensors and actuators) in industrial, technological and commercial applications, such as medical ultrasonic

[a.] Electronic Materials Research Laboratory, Key Laboratory of the Ministry of Education & International Center for Dielectric Research, School of Electronic Science and Engineering, Xi'an Jiaotong University, Xi'an, 710049, China. E-mails: liu.z.h@xjtu.edu.cn and gangniu@xjtu.edu.cn
[b.] Department of Applied Physics, Donghua University, Ren Min Road 2999, Songjiang, Shanghai, 201620, China
[c.] Department of Chemistry and 4D LABS, Simon Fraser University, Burnaby, British Columbia, V5A 1S6, Canada. E-mail: zye@sfu.ca

Zenghui Liu was born in Shaanxi, China, in 1990. He received the Ph.D. degree in Xi'an Jiaotong University, Xi'an, China, in 2017. From 2015 to 2017, he worked at the Department of Chemistry, Simon Fraser University, Burnaby, BC, Canada as a visiting Ph.D. student. Since 2018, he has been an assistant professor at Xi'an Jiaotong University. He has coauthored more than 30 research articles. His research interests include high-performance piezo-/ferroelectric single crystals, relaxor ferroelectrics, antiferroelectric materials, and their applications.

Gang Niu was born in Xi'an, China in 1982. He received the B.S. in and M.S. degrees from Xi'an Jiaotong University (XJTU) in 2004 and 2007, respectively. He obtained the Ph.D. degree from Ecole Centrale de Lyon France in 2010. He was a post-doctoral researcher at Insitut des Nanotechnologie de Lyon (INL) in CNRS France. From 2011 to 2015, he worked at Leibniz Insitute for high performance microelectronics (IHP) in Germany, firstly with the support of an Alexander von Humboldt fellowship then as a research scientist and a project leader. Since 2015, he has been a research professor at XJTU. He is the author of one book chapter, more than 90 journal papers. His research interests consist in ferroelectric oxides, epitaxy, and non-volatile memories etc. He holds eight patents and obtained Germany DFG Mercator fellowship in 2020.

Wei Ren received the B.Sc. and Ph.D. degrees from Xi'an Jiaotong University, Xi'an, China, in 1984 and 1992, respectively. He joined Xi'an Jiaotong University in 1987, where he was promoted to a professorship in 1997. He has held visiting appointments at Heinrich Hertz Institute, Berlin, Germany, from 1992 to 1993, Materials Research Laboratory, The Pennsylvania State University, University Park, PA, USA, from 1998 to 1999, and the Department of Physics, Royal Military College of Canada, Kingston, ON, Canada, from 1999 to 2004. He is currently the Chair Professor with the School of Electronic Science and Engineering, Xi'an Jiaotong University, where he is also the Director of the Institute of Ferro Materials and Integrated Devices and the Executive Director of the International Center for Dielectric Research. He has published more than 290 articles. He holds 30 Chinese and U.S. patents. His current research interests include piezoelectric and ferroelectric materials for sensor and transducer applications.

Hua Wu received her Ph.D. degree from Shanghai Jiaotong University Shanghai, China. She joined the faculty of Donghua University Shanghai, China, in 2006, and has been an associate professor since 2011. She was a visiting research professor at Simon Fraser University Burnaby, British Columbia, Canada (2013 to 2014, and 2016 to 2018) Dr. Wu's research interests include theoretical research on the phase transition phenomena, dielectric, piezoelectric and soft-mode behaviors in strained ferroelectric thin film; modeling and characterization of the structure and physical properties of nove multiferroics and (anti)ferroelectric materials of complex perovskite structure.

Jian Zhuang was born in Hunan, China, in 1988. He received the B.Sc and Ph.D. degrees in electronic science and technology from Xi'an Jiaotong University, Xi'an, China, in 2010 and 2015, respectively. From 2015 to 2018, he was a lecturer with Electronic Materials Research Lab Xi'an Jiaotong University, where he has been an associate professor with the School of Electronic Science and Engineering since 2019. His current research interests include single-phase multiferroics, relaxor ferroelectrics, piezoelectric single crystals, and dielectric spectra.
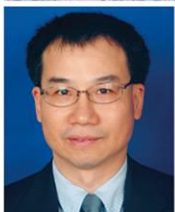
Zuo-Guang Ye received the Ph.D. degree from l'Université de Bordeaux Bordeaux, France, in 1988, followed by postdoctoral research at l'Université de Geneva, Geneva, Switzerland. He joined the faculty o Simon Fraser University (SFU), Burnaby, BC, Canada, in 1997, where he has been a Full Professor with tenure since 2003. He has been named a Distinguished SFU Professor since 2020. He was an Infotech Oulu Lecturer at the University of Oulu, Oulu, Finland, in 2010 and 2014. His research interests include the growth and characterization of high-performance piezoelectric and ferroelectric single crystals, multiferroic and magnetoelectric materials, lead-free piezoelectric and ferroelectrics and relaxor ferroelectricity and its microscopic mechanisms. He was a recipient of the IEEE Ultrasonics, Ferroelectrics, and Frequency Control Society's Ferroelectrics Achievement Award (2014) and the IEEE Robert E. Newnham Ferroelectrics Award (2019). He was elected as a fellow of the IEEE (2017) and a fellow of the Royal Society of Canada (2019).

diagnostics and therapy, undersea communication, structural health monitoring (SHM), active machine tool control, power generation, geological exploration, and petrochemistry. [1-5]

Due to the rapid development in the automobile industry, downhole oil industry, aerospace industry, etc., piezoelectric materials face serious challenges in terms of their operating environments, particularly at elevated temperatures. [2, 6-8] For instance, the working temperature of the piezoelectric sensors in automobiles (such as braking detectors and fuel and exhaust system monitors) can reach 300 °C for signal conditioning and activity control. In the downhole oil industry, many of the sensors need to be functional at temperatures over 200 °C in order to get high-resolution detecting images for deeper drilling. [7, 8] However, none of the currently available piezoelectric materials can fully satisfy the above-mentioned requirements.

Perovskite constitutes the largest structural family among piezo-/ferroelectric materials. It has a general formula of ABO_3 with the $Pm\overline{3}m$ space group at high temperatures (See Fig. 1(a1)). As a typical representative of perovskite piezoelectrics, lead zirconate-titanate solid solution $PbZr_{1-x}Ti_xO_3$ (PZT) ceramics with compositions near the morphotropic phase boundary (MPB) exhibit good electromechanical performance at room temperature. Here MPB refers to an almost temperature-independent phase boundary (or region) where different phases coexist, and it is known that the piezoelectric and dielectric responses typically peak around the MPB compositions in PZT and other piezo-/ferroelectric solid solutions. [1, 3, 13, 14] However, PZT ceramics suffer from serious

depoling and aging problems at temperatures above 150 °C, which greatly limits their working performance at elevated temperatures. [1] Though some none-perovskite piezoelectric materials, such as $PbNb_2O_6$ and $LiNbO_3$, show piezoresponse at higher temperatures, their piezoelectricity is generally very weak. [6] As a result, the sensing and actuating capabilities of the electromechanical transducers made of these materials are rather mediocre. Thus, it is vital to develop new piezoelectric materials that are suitable for high-temperature electromechanical applications.

In the last decade, bismuth-based piezo-/ferroelectric materials of complex perovskite structure have attracted intense attention due to their high Curie temperature (T_C), good piezoelectricity, less toxicity, etc. Such materials have proved to be a promising family of novel piezoelectrics for high-temperature electromechanical applications, which are superior to the conventional lead-based piezoelectric materials, such as PZT and $Pb(Mg_{1/3}Nb_{2/3})O_3$-$PbTiO_3$ (PMN-PT). [3, 13, 14] In particular, in recent years, successful growth and subsequent characterization of bismuth-based piezo-/ferroelectric single crystals (BPSCs) have not only made these materials available with significantly enhanced piezoelectricity, but also deepened our understanding of this family of materials from fundamental aspects. In this highlight, recent progress in the development and understanding of BPSCs is reviewed in terms of materials design, crystal growth, piezo-/ferroelectric properties, crystal chemistry and complex domain structures. The future perspectives of BPSCs are also discussed.
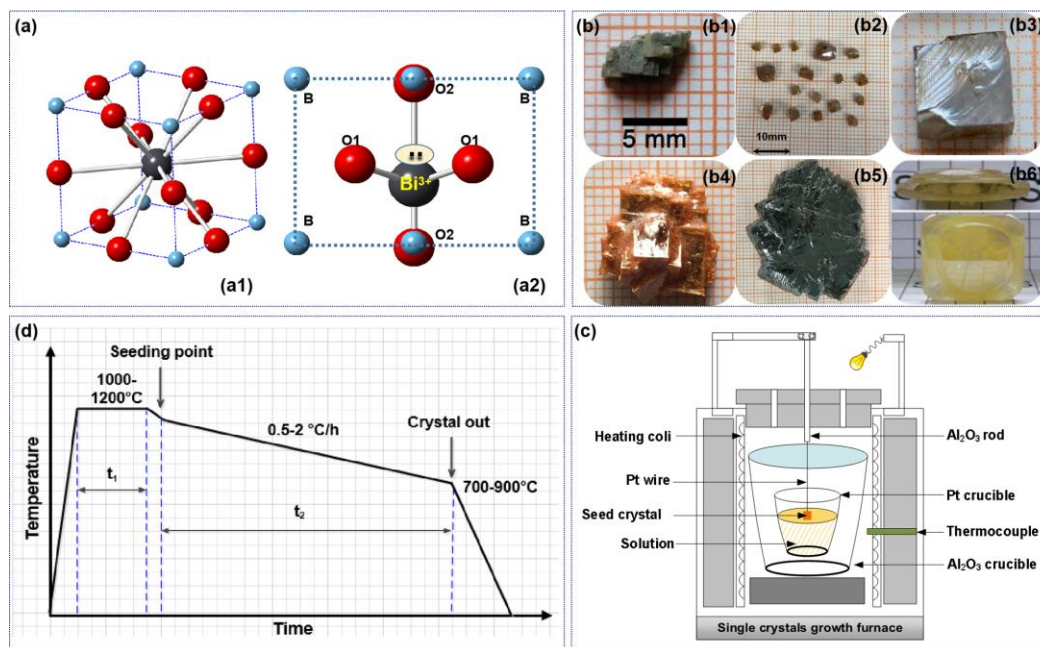
Fig. 1. Structure and crystal growth of BPSCs. (a) The perovskite structure: (a1) The ideal perovskite structure with the $Pm\overline{3}m$ space group. (a2) The projection on the (110) plane of a distorted perovskite, depicting the anisotropic Bi-O bond lengths resulting from the stereochemically active lone electron pair on Bi^{3+}. (b) Selected as-grown BPSCs: $BiScO_3$-$PbTiO_3$ single crystals grown by (b1) the flux method and (b4) the top-seeded solution growth method, respectively; $Bi(Zn_{2/3}Nb_{1/3})O_3$-$PbTiO_3$ single crystals grown by (b2) the flux method and (b5) the top-cooled solution growth method, respectively; (b3) $Bi(Mg_{1/2}Ti_{1/2})O_3$-$PbTiO_3$ single crystals grown by the flux method and (b6) $(Na_{1/2}Bi_{1/2})TiO_3$-$BaTiO_3$-$(K_{1/2}Na_{1/2})NbO_3$ single crystals grown by the top-seeded solution growth method. (c) Furnace and crucible setup for the top-seeded solution growth. (d) Typical temperature profile used for the crystal growth. Reproduced with permission from Ref. 9 (Copyright 2020 by the Royal Society of Chemistry), Ref. 10 (Copyright 2017 by Elsevier), Ref. 11 (Copyright 2015 by the Royal Society of Chemistry) and Ref. 12 (Copyright 2020 by Wiley).

2. Lone-pair ($6s^2$) electrons and their effects on piezo-/ferroelectric properties

Both the Bi^{3+} and Pb^{2+} ions have the same electronic configuration of $[Xe]4f^{14}5d^{10}6s^2$, containing $6s^2$ lone-pair electrons in the outermost electron shell. A pair of electrons that does not take part directly in chemical bonding is defined as a lone pair. In bismuth/lead-based piezo-/ferroelectric materials, the $6s^2$ lone pair electrons are stereochemically active due to the *sp* hybridization between the orbitals of Bi^{3+}/Pb^{2+} and oxygen anion. [15] Generally, the lone-pair repulsive force applied to other bonding schemes impacts the spatial distribution of the bonding electron pairs, leading to an asymmetric local coordination environment (Fig. 1(a2)). As a result, a non-centrosymmetric and polar crystal structure will be induced, leading to enhanced physical properties, especially piezoelectricity and ferroelectricity. [15-18] A comparative study of $PbTiO_3$ (PT) and $BaTiO_3$ shows that PT possesses stronger ferroelectricity with a much higher T_C than $BaTiO_3$ does (~ 495 °C for PT and ~ 130 °C for $BaTiO_3$) [1], which is to a large extent due to the effects of the stereochemically active $6s^2$ lone-pair electrons on Pb^{2+}. [19] Hence, ions with lone-pair electrons, such as Bi^{3+} and Pb^{2+}, play a crucial role in enhancing the physical properties of piezo-/ferroelectric materials.

Compared with lead and other heavy metals, bismuth is less toxic; the lethal intake level of lead is 1 mg for a 70 kg human, whereas that of bismuth is 15×10^3 mg. [20] In addition, Bi^{3+} has a smaller ionic radius (1.36 Å) compared with that of Pb^{2+} (1.49 Å), allowing for a larger ionic displacement in the oxy-octahedron of the unit cell. As a consequence, a larger crystal distortion (polarization) can be induced in bismuth-based perovskite, which is beneficial to high piezo-/ferroelectricity and high T_C. However, the smaller Bi^{3+} makes many bismuth-based perovskites less stable and more difficult to be synthesized unless under very high pressure. [21] To solve this problem, other stable perovskites (such as PT) have been used as host to form complex solid solutions, effectively stabilizing the phase of bismuth-based perovskites. This method also serves as a viable approach for designing new piezo-/ferroelectric single crystals with better performance.

3. Growth of BPSCs

Growth of BPSCs has been a challenge for a long period of time due to the nature of their chemical instability at high temperatures and the lack of knowledge on relevant phase diagrams and optimum growth conditions. [21] In recent years, by the trial-and-error approach, several BPSCs of complex perovskite solid solution systems have been successfully grown by the flux method despite their mostly incongruent (or peritectic) melting behaviour, and the size and quality of the as-grown single crystals have been further improved by the top-cooled and top-seeded solution growth methods. [9-12, 22-33]

3.1 Flux growth

The flux growth method (also called high-temperature solution growth method) is a versatile technique to grow piezo-/ferroelectric crystals with complex perovskite structure. The principle of flux growth is based on the spontaneous nucleation that occurs when supersaturation is reached upon slow cooling of a high temperature solution. [34] In earlier studies, one of the major issues in growing PBSCs was the control of spontaneous nucleation, which was partially due to the lack of reliable crystal growth parameters. As a result, the as-grown crystals typically contained a large amount of flux inclusions, cleavage planes, and dendrites, and were relatively small in size. [24, 35, 36]

In recent investigations, the growth conditions (especially the flux composition) were gradually optimized, which has improved the quality of the crystals and their sizes to some extent (Fig. 1(b)). Table 1 summarizes the fluxes used to grow the different BPSCs. The as-grown crystals can be grouped into two categories according to their compositions, i.e., the solid solutions with PT and the lead-free systems.

To grow the crystals of the solid solutions with PT, a complex flux, i.e., PbO/Pb_3O_4 with a suitable amount of Bi_2O_3, is a good selection for the following reasons: i) the $PbO/Pb_3O_4+Bi_2O_3$ system has relatively low melting temperatures; ii) the flux is effective in dissolving the refractory oxides because of the high polarizability of the Bi^{3+} and Pb^{2+} ions; and iii) both PbO/Pb_3O_4 and Bi_2O_3 are constituent oxides of the solute and thus can prevent the introduction of impurities in the grown crystals. [5, 34] The studies have shown that an important step in the growth of lead-containing BPSCs with desirable compositions, especially in the MPB region, is the control of the composition of the solute and the selection of the flux, especially the amount of Bi_2O_3 as additive. Due to the high volatility of Bi_2O_3 at elevated temperatures, an insufficient amount of Bi_2O_3 would lead to bismuth-deficiency in the crystals, making the crystal composition and structure shift to the PT-rich side. On the other hand, an overly excess amount of Bi_2O_3 would increase the

Table 1. Complex flux used for the growth of various bismuth-containing perovskite single crystals

As-grown single crystals	Flux used	Size (mm)	Refs.
Solid solutions with PT:			
$BiScO_3$-$PbTiO_3$	$PbO/Pb_3O_4+Bi_2O_3$	3-8	9, 22
$Bi(Zn_{1/2}Ti_{1/2})O_3$-$PbTiO_3$	$PbO+B_2O_3$	~5	10
$Bi(Mg_{1/2}Ti_{1/2})O_3$-$PbTiO_3$	$PbO/Pb_3O_4+Bi_2O_3$	2-10	11, 23
$Bi(Zn_{2/3}Nb_{1/3})O_3$-$PbTiO_3$	$PbO+B_2O_3$	~15	10
$BiFeO_3$-$PbTiO_3$	$PbO/Pb_3O_4+Bi_2O_3$	~2	24, 25
$BiScO_3$-$PbTiO_3$-$Pb(Cd_{1/3}Nb_{2/3})O_3$	$PbO+Bi_2O_3+B_2O_3$	2-4	26, 38
$BiScO_3$-$PbTiO_3$-$BiGaO_3$	$Pb_3O_4+Bi_2O_3$	3-8	27
$Bi(Zn_{1/2}Ti_{1/2})O_3$-$PbZrO_3$-$PbTiO_3$	$PbO+H_3BO_3$	~20	28, 29
$Bi(Zn_{1/2}Ti_{1/2})O_3$-$PbTiO_3$-$Pb(Mg_{1/3}Nb_{2/3})O_3$	$PbO+H_3BO_3$	5-14	30
$Bi(Zn_{2/3}Nb_{1/3})O_3$-$PbTiO_3$-$Pb(Mg_{1/3}Nb_{2/3})O_3$	$PbO+B_2O_3$	5-20	31
Lead-free systems:			
$(Bi_{1/2}Na_{1/2})TiO_3$	$Bi_2O_3+Na_2CO_3$	5-45	37
$(Bi_{1/2}Na_{1/2})TiO_3$-$BaTiO_3$	$Bi_2O_3+Na_2CO_3$	~10	32
$(Bi_{1/2}Na_{1/2})TiO_3$-$BaTiO_3$-$(K_{1/2}Na_{1/2})NbO_3$	$Bi_2O_3+Na_2CO_3+K_2CO_3$	10-35	12
$(Bi_{1/2}Na_{1/2})TiO_3$-$Bi(Zn_{1/2}Ti_{1/2})O_3$	$Bi_2O_3+Na_2CO_3$	12-35	33

system instability, preventing the growth of the perovskite crystals. Note that the subtle amount of Bi_2O_3 additive in the flux is system-dependent.

The growth of lead-free BPSCs has mainly focused on the $(Bi_{1/2}Na_{1/2})TiO_3$ (BNT)-based systems. BNT melts congruently, making it relatively easier to grow single crystals. [37] However, due to the volatilization of Bi_2O_3 and Na_2O during the crystal growth process, a complex flux based on $Bi_2O_3+Na_2CO_3$ is recommended in order to achieve the stoichiometry in the as-grown crystals. [12, 32, 33, 37]

3.2 Top-cooled and top-seeded solution growths

To grow BPSCs with a larger size and better quality, the top-cooled solution growth (TCSG) and top-seeded solution growth (TSSG) methods were developed. [10, 12, 26] For TCSG, a platinum wire is hung on the top of the high temperature solution. Due to its excellent thermal conductivity, a temperature gradient is created on the platinum wire and thereby the nucleation is triggered around the tip of the wire slightly submerged in the solution. In the TSSG growth, a seed crystal is attached to an end of a platinum wire and submerged into the top layer of the solution. The crystal can grow epitaxially around the seed crystal without constrain, which is beneficial to grow large single crystals with well-developed morphology and desired orientation. This technique is different from the bottom-seeded method in which the growth occurs on the bottom of the crucible surrounding the seed due to a reverse temperature gradient. In addition, both the TCSG and TSSG methods can enhance the transport of solute by convection, resulting in a more homogenous composition. [5] Fig. 1(c) and (d) show the experimental setup of the TSSG and the typical temperature profile, respectively, used for the growth of BPSCs. Using the optimized conditions determined from the flux growth method, BPSCs of large size and high quality have been successfully grown, as shown in Fig. 1(b4), (b5) and (b6). [10, 12, 39]

4. Properties of BPSCs

Many of the BPSCs exhibit excellent piezo-/ferroelectric properties and a relatively high T_C, making them very promising candidates for high-temperature electromechanical transduction applications. In this section, the properties of BPSCs are discussed according to their compositions, i.e., the solid solutions with PT and the lead-free systems.

4.1 Solid solutions with PT

As a stable perovskite with good piezo-/ferroelectricity and a high T_C (~ 495 °C), PT is one of the best end-members to form solid solutions with bismuth-based perovskites. [1, 5] Interestingly, in some systems, the T_C of PT can be further enhanced when forming solid solutions with bismuth-based perovskites. [10, 11, 25, 40-42] For example, the $Bi(Zn_{1/2}Ti_{1/2})O_3-PbTiO_3$ (BZT-PT) solid solution single crystals show a T_C up to 572 °C, which is much higher than that of relaxor-PT crystals. [10] The enhanced T_C is mainly caused by the partial substitutions of bismuth for lead on the A-site and ferroelectrically active cation(s) for titanium on the B-site, which will be discussed in Sec. 5.1. Therefore, the bismuth-based perovskites are excellent components to form new piezo-/ferroelectric materials with enhanced T_C.

More importantly, due to the high T_C in bismuth-based perovskites, a high-temperature MPB can exist when forming solid solutions with PT, which is advantageous for achieving excellent piezoelectric performance in a wide temperature range. For example, excellent and stable piezoresponse up to high temperatures have been found in materials like $BiScO_3-PbTiO_3$ (BS-PT), $Bi(Mg_{1/2}Ti_{1/2})O_3-PbTiO_3$ and $BiFeO_3-PbTiO_3$. [22, 23, 25, 42-44] Among the systems so-far developed, the performance of BS-PT single crystals appears to be the most outstanding. Table 2 lists the orientations, symmetries, and physical properties of BS-PT single crystals with different compositions. A high piezoelectric coefficient ($d_{33} \approx 1150$ pC/N) has been achieved in the <001>-oriented rhombohedral BS-PT crystal with composition near the MPB region, and particularly, it shows a much higher T_C (402 °C), a higher rhombohedral to tetragonal (or morphotropic) phase transition temperature (T_{RT} = 349 °C) and a larger coercive field (E_C = 14 kV/cm) compared with those of the relaxor-PT crystals. [13, 22, 45, 46] Therefore, BPSCs are attractive candidates for high-temperature, high-power, and high-performance electromechanical applications as sensors and actuators, overcoming the drawbacks of the relaxor-PT crystals.

4.2 Lead-free BPSC systems

Table 2. Orientations, symmetries, and physical properties of BS-PT single crystals with different compositions near the MPB region. The properties of different relaxor-PT piezo-/ferroelectric crystals are listed for comparison. "T", "R" and "MPB" in the "Structure" column stand for the tetragonal symmetry, the rhombohedral symmetry and the morphotropic phase boundary, respectively.

Composition	Structure	Orientation	T_C (°C)	T_{RT} (°C)	d_{33} (pC/N)	k_{33}	P_r ($\mu C/cm^2$)	E_C (kV/cm)	Ref.
0.34BS-0.66PT	T	<001>	460	/	200	0.73	28	34	35
0.37BS-0.63PT	MPB	<001>	443	350	900	/	43	20	36
0.37BS-0.63PT	MPB	<110>	440	325	350	/	34	24	36
0.37BS-0.63PT	MPB	<111>	445	307	200	/	36	27	36
0.43BS-0.57PT	R	<001>	402	349	1150	0.90	23	14	22
PMN-PT	MPB	<001>	96	135	2100	0.91	27	2.2	45
Sm-PMN-PT	MPB	<001>	120	50	4100	0.95	23	2.5	13
PIN-PMN-PT	MPB	<001>	197	96	2742	0.95	34	5.5	46

Table 3. Crystal structure and physical properties of the <001>-oriented BNT-based lead-free BPSC systems. "R" and "MPB" in the "Structure" column stand for the rhombohedral symmetry and the morphotropic phase boundary, respectively.

Material system	Structure	T_C (°C)	d_{33} (pC/N)	P_r ($\mu C/cm^2$)	E_C (kV/cm)	Ref.
$(Bi_{1/2}Na_{1/2})TiO_3$-BaTiO_3	MPB	/	420	11.8	22	47
Fe-$(Bi_{1/2}Na_{1/2})TiO_3$-BaTiO_3	MPB	/	590	53.2	35	47
$(Bi_{1/2}Na_{1/2})TiO_3$-BaTiO_3-$(K_{1/2}Na_{1/2})NbO_3$	MPB	271	840	/	/	12
$(Bi_{1/2}Na_{1/2})TiO_3$-Bi$(Zn_{1/2}Ti_{1/2})O_3$	R	339	121	21.5	60	33

To prevent the toxicity of lead, lead-free BPSCs have been developed, which provides a workable solution to partially replace the currently used lead-based piezoelectric materials. Among the lead-free BPSCs, the BNT-based crystals are most extensively investigated due to the possibility to grow large-size and high-quality single crystals. [12, 33, 47] Table 3 lists the structure and physical properties of the <001>-oriented BNT-based lead-free single crystals. Although the T_Cs of lead-free BPSCs are generally lower than those of lead-containing BPSCs, they are still much higher than those of relaxor-PT piezoelectric crystals. [13, 45, 46] Therefore, the lead-free BPSCs are also viable materials for high-temperature electromechanical applications, especially when lead content is strictly untolerated.

5. Crystal chemistry and domain structures in BPSCs

The high T_C and excellent electric properties found in BPSCs have prompted intensive research work on the crystal chemistry and domain structures of this family of materials. In this section, the current understanding of the origin of the high T_C, the crystal structure, and the complex domain structures in the MPB and the tetragonal phase regions are highlighted.

5.1 Origin of the high T_C in BPSCs

A notable feature of BPSCs is their high T_C, which makes them promising candidates for high-temperature electromechanical applications. In general, T_C is a measure of the thermal stability of the asymmetric and polar structure in ferroelectric materials. The high T_C of BPSCs can be attributed to the very large structural distortion and the associated polarization according to recent studies.

One of the major reasons leading to the large distortion/polarization is the unique crystal chemistry feature of the A-site cations (especially the bismuth). In the BPSCs of solid solutions with PT, the A site of perovskite is occupied by the Bi^{3+} and Pb^{2+} ions, which, due to the existence of the lone-pair electrons on them, result in exceptionally large distortions and thereby high T_C. Such an effect becomes more prominent
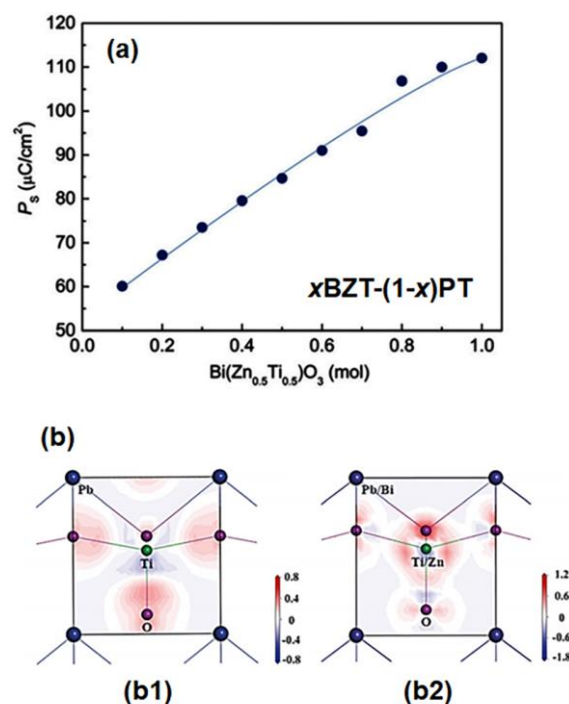
Fig. 2. The structural mechanism of high T_C and large polarization in the BZT-PT system. (a) The spontaneous polarization of BZT-PT as a function of BZT concentration. (b) The electron density difference map of (b1) PT and (b2) 0.5BZT-0.5PT, indicating the enhancement of the orbital hybridization by the partial Bi - Pb and Zn - Ti substitutions. Reproduced with permission from Ref. 40 (Copyright 2018 by the Royal Society of Chemistry).

when the concentration of bismuth is higher. The first-principles calculations show that the large polarization of BS-PT is dominated by the strong hybridization between the Pb/Bi-6p and O-2p orbitals, which is enhanced by the substitution of Bi for Pb. [48] The beneficial effect of bismuth was further confirmed by neutron powder diffraction, which indicates that both the polarization and T_C are significantly enhanced by introducing bismuth into the crystal lattice of BS-PT. [49] In lead-free BPSCs, due to the diluted amount of lone-pair electrons, T_Cs are generally lower, as shown in Table 3.

In addition to the contribution of bismuth on the A-site, B-site cations also play a critical role owing to the coupling effect between the A-site and B-site cations. [50] For example, the BZT-PT system shows enhanced T_C and polarization (Fig. 2(a)) with increasing BZT concentration. [10, 40] Theoretical analysis suggests that the high T_C and large structural distortions in BZT-PT arise from the hybridization between the empty 4s and 4p orbitals of Zn^{2+} and the O^{2-} 2p orbitals (See Fig. 2(b)) that enables a favourable coupling effect between the A-site and B-site displacements. [40, 51] The coupling effect was experimentally evidenced by the structural refinements which reveal an ultralarge tetragonal distortion accompanied with both large A-site and B-site off-center displacements (up to ~ 0.5 Å) in BZT-PT. [10] As a result, the normally oxy-octahedral coordination of B-site ions becomes a pyramidal coordination. [40]

Therefore, the high T_C and large polarization in BPSCs arise from the unique crystal chemistry feature of bismuth and the related coupling effects of A-site and B-site cations.
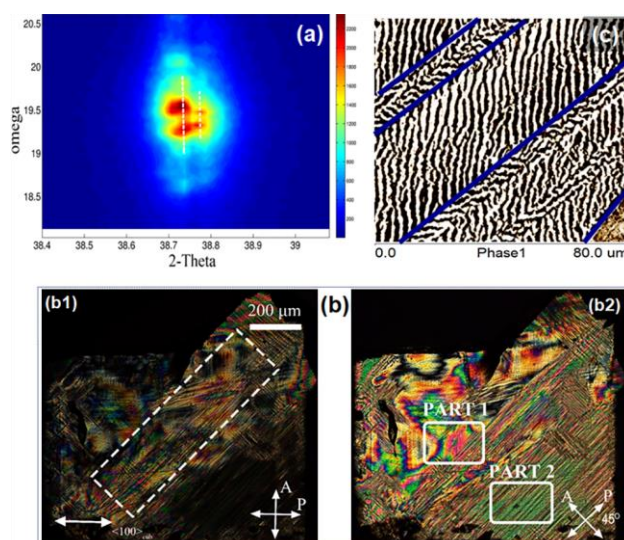
Fig. 3. The morphotropic crystal structure and domain structure in BPSCs. (a) the ω-2ϑ reciprocal space mapping (RSM) image of the 0.40BiScO₃-0.05Pb(Cd₁/₃Nb₂/₃)O₃-0.55PbTiO₃ (0.40BS-0.05PCN-0.55PT) single crystal for the {111} reflection, indicating the existence of the monoclinic phase in the MPB region. (b) Ferroelastic domain structure of a <001>-orientated 0.40BS-0.05PCN-0.55PT single crystal platelet observed by PLM with crossed polarizers parallel (b1), and at 45° (b2), to the <100>cub direction, respectively. The non-complete extinction behaviour (marked by a dashed white rectangle) shown in Fig. 3(b1) indicates the monoclinic symmetry of the crystal. Two kinds of domain arrangements (represented by Part 1 and 2 in Fig. 3(b2)) are observed. Fine domains with a high domain wall density are observed (Part 2 of Fig. 3(b2)). (c) Out-of-plane PFM phase images of the 0.4BS-0.05PCN-0.55PT crystals. The area was selected from Part 2 of Fig. 3(b2). The contrast of colour in the image reveals different polarization directions, and the blue lines indicate the ferroelastic domain boundaries. Reproduced with permission from Ref. 26 (Copyright 2018 by the Royal Society of Chemistry).

5.2 Complex morphotropic structures at the MPB

5.2.1 Monoclinic phase at the MPB. Associated with their high T_C, bismuth-based perovskite solid solutions that exhibit excellent piezoelectric performance typically possess a morphotropic phase boundary region that extends to elevated temperatures (typically > 300 °C), i.e. a high-temperature MPB. In the MPB region, different phases, such as rhombohedral, tetragonal and monoclinic phases, coexist as they have similar Gibbs free energy landscapes. [1, 5] In BS-PT, a monoclinic phase was found to coexist with the rhombohedral and/or tetragonal phase in the MPB region. However, the exact phase nature of the MPB is still under debate. A tetragonal phase (*P4mm* space group) and a monoclinic M_A phase (*Cm* space group) were found to coexist in the MPB region and their phase component changes under the application of an electric field. [52-57] On the other hand, recent high-resolution single crystal X-ray diffraction results suggest the existence of two primitive monoclinic lattices (space group *Pm*) in the MPB region. [58] Moreover, a monoclinic phase was not only found at the MPB region but also in the well-established tetragonal phase region (0.39 ⩽ x ⩽ 0.40). [59] A systematical investigation performed recently on the BS-PT-based system clearly indicates the existence of the monoclinic

phase with *Pm* space group in the MPB region (See Fig. 3(a)). [26] More detailed crystallographic studies are needed to achieve a better understanding of the complex MPB structures of BPSC.

5.2.2 Monoclinic domain structures. The electromechanical properties of a piezoelectric crystal are closely determined by its domain structure. [60, 61] Analysis and understanding of the domain structure of BPSCs is essential for establishing the relationship between the meso-/nanoscopic domain structure and the macroscopic properties. Due to the complicated crystallographic features in the MPB region, the corresponding domain structure in BPSCs appears to be rather complex.

The monoclinic domains in the BPSCs of MPB compositions have been observed and analyzed by polarized light microscopy (PLM) based on the optical crystallography and group/subgroup symmetry relation. [31, 62, 63] Under PLM, the ferroelastic domain structure of the monoclinic phase can be determined by analyzing the characteristic extinction behaviors of the crystal. A salient feature of the BS-PT-based piezoelectric single crystals with MPB composition is the coexistence of different ferroelastic domain arrangements as shown in Fig. 3(b). In addition, the crystals show fine and superimposed domain structures with a high domain wall density. [12, 26, 31] Noticeably, the crystal does not extinct either parallel, or at 45°, to the <100>cub direction, indicating the monoclinic symmetry. [26]

The ferroelectric polar domains of the BS-PT-based single crystals on the nanoscale were revealed by piezoresponse force microscopy (PFM) by analyzing the in-plane/out-of-plane piezoresponse amplitude and phase imaging. [64, 65] The PFM investigations not only confirm the existence of the monoclinic phase in the MPB region, but also indicate the distinct feature of the crystals, that is, only the MPB crystals display a variety of ferroelastic domains with fingerprint-like ferroelectric domains (~ 1 µm in width) embedded in them (See Fig. 3(c). [26] Such character was also found in PZT and relaxor-PT systems, but differently, the ferroelectric domain sizes in PZT and relaxor-PT piezoelectric crystals are much smaller (on nanometer scale). [5, 31, 66, 67]

The excellent piezoelectric properties in the BS-PT-based piezo-/ferroelectric single crystals are closely related to the effects of MPB where the polarization rotation is facilitated. Especially, the existence of the monoclinic phase in the MPB region acts as a structural bridge, provides additional polarization/domain states and makes the crystals electrically active, leading to high electromechanical response. [31, 68, 69]

5.3 Domain configurations in tetragonal crystals

In addition to the complex domain structures in the MPB region, the domain configurations of tetragonal BPSCs also appear to be intriguing. Two different types of domains belonging to this category have been found.

5.3.1 Micro- to nanoscale domains. Although only two types of domains, i.e., 90°and 180° domains (*a*-domains and *c*-domains) can be formed in a tetragonal ferroelectric perovskite crystal, complicated domain structures have been observed in BPSCs of tetragonal symmetry. This domain structural complexity arises
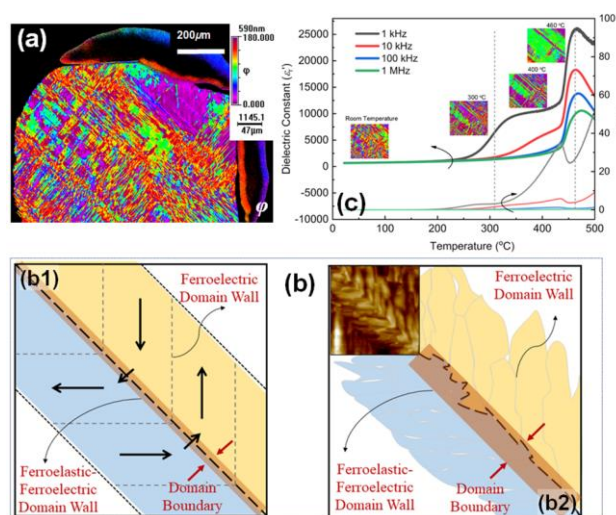
Fig. 4. The micro- to nanoscale domains in the tetragonal BS-PT single crystals. (a) The orientation image in BS-PT obtained from the birefringence imaging microscopy measurement, indicating the small domain size and the local crystal distortion (φ value in between 0° and 180°). (b) Schematics of the 90° domain boundaries: (b1) Ideal polarizations in the domains and domain boundaries are shown schematically by thick arrows, while the brown stripe stands for the domain boundary. (b2) Schematics of the polarizations in the BS-PT crystal based on the topography image (inset) of PFM measurements, showing the distorted structure near the ferroelastic/ferroelectric domain boundary. (e) The temperature dependences of dielectric constant and loss tangent of the BS-PT crystal, together with the domain structures at selected temperatures. Reproduced with permission from Ref. 9 (Copyright 2020 by the Royal Society of Chemistry).

Fig. 5. The ferroelastic/ferroelectric monodomain state of a tetragonal 0.35BS-0.05PCN-0.60PT single crystal. (a) Temperature profile used to grow the single crystals. Inset shows the crystal used for PLM and PFM investigations. (b) Schematic indicating the orientations of the crystal. (c) PLM images under crossed polarizer (P) and analyzer (A) which are parallel (c1 and c2), and at 45° (c3 and c4), to the <100> direction, observed at room temperature on the (001) (c1 and c3) and (100) (c2 and c4) faces, respectively. The PLM images indicate a mono-ferroelastic domain state. (d) Out-of-plane ([001] direction) PFM phase images (d1) in the virgin state and (d2) after application of a +30 V (on the outer 12 × 12 μm^2 square) and then a -30 V (on the inner 4 × 4 μm^2 square) DC tip biases. No ferroelectric domain walls can be observed in the virgin state, indicating a homogenous mono-ferroelectric domain state. (d2) reveals that the polarizations are switchable under electric fields. Reproduced with permission from Ref. 39 (Copyright 2020 by the Royal Society of Chemistry).

from the micro- to nanoscale domains which interplay with each other. The sizes of ferroelectric/ferroelastic domains found in BPSCs vary from a few hundred nanometers to several micrometers. [9, 70-72] For example, in tetragonal BS-PT single crystals, ferroelastic/ferroelectric domains of 2 - 3 μm size were observed [9], which are significantly smaller than those found in conventional tetragonal crystals such as PT, [73] indicating that stronger internal stresses exist in the crystal upon cooling through T_C. The internal stresses cause great local distortions in the crystal (Fig. 4(a)), and lead to much broader (200 - 300 nm) ferroelastic/ferroelectric domain boundaries (Fig. 4 (b)) compared with those observed in other ferroelectric single crystals (~ 20 nm). [74, 75] Similar features were also found in the Bi(Zn$_{2/3}$Nb$_{1/3}$)O$_3$-PbTiO$_3$ (BZN-PT) single crystal of tetragonal symmetry (with a high T_C of 430 °C), but the domain sizes in BZN-PT single crystals vary from several tens of nanometers to a few micrometers. [70]

The above-mentioned micro- to nanoscale domains are closely related to the electric properties of BPSCs. In the BS-PT crystals, due to the highly active domains with small sizes, the dielectric constant and loss change significantly with the domain structure (Fig. 4(c)), indicating a strong correlation between the dielectric properties and the domain structures. [9]

5.3.2 Ferroelastic/ferroelectric monodomain state. In addition to the complex polydomain structures, ferroelastic/ferroelectric monodomains (of several millimeters in size) were also found in BPSCs. [39] A monodomain state is not very common, as a

polydomain state is energetically more favourable to form to meet the mechanical and electrical compatibility principles. [61] Interestingly, by the TSCG method using the temperature profile in Fig. 5(a), BS-PT-based piezo-/ferroelectric single crystals with a ferroelastic/ferroelectric monodomain structure have been successfully grown. The monodomain state is revealed by PLM and PFM imaging as shown in Fig. 5(b-d). These crystals show a self-polarized state with an excellent temperature stability, proving to be a promising candidate for both fundamental research and technological applications. [39]

The reason(s) for the formation of such a unique domain structure remains to be understood. A possible mechanism is that anisotropic mechanical stress that is developed during the TSSG "poles" the crystal into a preferred orientation state with a single ferroelastic domain when the crystal undergoes the ferroelastic/ferroelectric phase transition upon cooling.

6. Concluding remarks and future perspective

Significant progress has been made in recent years in the development of bismuth-based piezo-/ferroelectric single crystals (BPSCs), especially in terms of crystal growth, physical properties, crystal chemistry, and domain structures. BPSCs have become an attractive family of materials exhibiting both high T_C and excellent piezo-/ferroelectric performance. They

CrystEngComm

are promising materials for high-temperature and high-power electromechanical transduction applications.

The ongoing and future research work on BPSCs mainly focuses on the following three aspects: i) optimize the crystal growth parameters and processes, ii) improve the dielectric properties, and iii) design and fabricate novel transducers.

The growth of high-quality and large-size BPSCs with desirable compositions is still a challenging task. More detailed investigations on the chemical, thermodynamic and kinetic factors and their effects on the growth results are crucial for determining the optimum growth conditions. Especially, establishment of the relevant phase diagrams of the related multi-component systems is essential to determine the melting behaviour and to find optimum conditions for growing BPSCs of desired compositions with chemical stoichiometry. In particular, systemic studies should be carried out to establish the correlation between growth parameters, chemical compositions and physical properties of BPSCs. Additionally, different growth techniques, such as bottom-seeded growth and modified Bridgman growth, need to be developed for the fabrication of BPSCs on large scale as a commercially available resource for applications.

Though BPSCs show excellent piezo-/ferroelectric properties with a good thermal stability, they suffer from relatively high dielectric losses at high temperatures and relatively low mechanical quality factors. Chemical modifications need to be carried out to further enhance the performance of the materials.

Design and fabrication of sensors and actuators using BPSCs will lead to novel electromechanical devices with better sensing and actuating capabilities and a broader operating temperature range for critical applications in such sectors as automobile, energy and aerospace.

Author Contributions

ZL and ZGY initiated the project. All the authors contributed to the collection, sorting and analysis of the literature data, and discussed the contents and presentation of the paper. ZL wrote the draft manuscript. ZL, GN, HW, JZ and ZGY revised and finalized the manuscript.

Conflicts of interest

There are no conflicts to declare.

Acknowledgements

References

1   B. Jaffe, C. William and H. Jaffe, *Piezoelectric ceramics*, Academic Press, London, 1971.
2   S. Trolier-McKinstry, S. Zhang, A. J. Bell and X. Tan, *Ann. Rev. Mater. Res.*, 2018, **48**, 191-217.
3   S. Zhang, F. Li, F. Yu, X. Jiang, H.-Y. Lee, J. Luo and T. R. Shrout, *J. Korean Cera. Soc.*, 2018, **55**, 419-439.
4   Q. Xu, X. Gao, S. Zhao, Y. N. Liu, D. Zhang, K. Zhou, H. Khanbareh, W. Chen, Y. Zhang and C. Bowen, *Adv. Mater.*, 2021, **33**, e2008452.
5   Z.-G. Ye, ed., *Handbook of advanced dielectric, piezoelectric and ferroelectric materials: Synthesis, properties and applications*, Woodhead Publishing, Cambridge, U.K., 2008.
6   S. Zhang and F. Yu, *J. Am. Ceram. Soc.*, 2011, **94**, 3153-3170.
7   X. N. Jiang, K. Kim, S. J. Zhang, J. Johnson and G. Salazar, *Sensors*, 2014, **14**, 144-169.
8   J. Wu, X. Gao, J. Chen, C.-M. Wang, S. Zhang and S. Dong, *Acta Phys. Sin-ch. Ed.*, 2018, **67**, 207701.
9   Z. Luo, Z. Liu, D. Walker, S. Huband, P. A. Thomas, N. Zhang, W. Ren and Z.-G. Ye, *J. Mater. Chem. C*, 2020, **8**, 7234-7243.
10 Z. Liu, H. Wu, A. Paterson, Z. Luo, W. Ren and Z.-G. Ye, *Acta Mater.*, 2017, **136**, 32-38.
11 J. Liu, X. Chen, G. Xu, D. Yang, Y. Tian and X. Zhu, *CrystEngComm*, 2015, **17**, 5605.
12 Y. Wang, C. Luo, S. Wang, C. Chen, G. Yuan, H. Luo and D. Viehland, *Adv. Electron. Mater.*, 2020, **6**, 1900949.
13 F. Li, M. J. Cabral, B. Xu, Z. Cheng, E. C. Dickey, J. M. LeBeau, J. Wang, J. Luo, S. Taylor, W. Hackenberger, L. Bellaiche, Z. Xu, L.-Q. Chen, T. R. Shrout and S. Zhang, *Science*, 2019, **364**, 264-268.
14 S.-E. Park and T. R. Shrout, *J. Appl. Phys.*, 1997, **82**, 1804-1811.
15 A. Walsh, D. J. Payne, R. G. Egdell and G. W. Watson, *Chem. Soc. Rev.*, 2011, **40**, 4455-4463.
16 D. SCHÜTZ and K. REICHMANN, *J. Ceram. Soc. Jpn.*, 2014, **122**, 231-236.
17 G. H. Olsen, M. H. Sørby, S. M. Selbach and T. Grande, *Chem. Mater.*, 2017, **29**, 6414-6424.
18 E. S. Claudio, H. A. Godwin and J. S. Magyar, *Journal*, 2003, **34**, 1-144.
19 R. E. Cohen, *Nature*, 1992, **358**, 136-138.
20 R. Wang, H. Li and H. Sun, *Encyclopedia of Environmental Health (Second Edition)*, 2019, 415-423.
21 A. A. Belik, *J. Solid State Chem.*, 2012, **195**, 32-40.
22 S. Zhang, C. A. Randall and T. R. Shrout, *Appl. Phys. Lett.*, 2003, **83**, 3150-3152.
23 Y. Tian, G. Xu, J. Liu and X. Zhu, *Solid State Commun.*, 2016, **245**, 50-54.
24 W.-M. Zhu, H.-Y. Guo and Z.-G. Ye, *J. Mater. Res.*, 2007, **22**, 2136-2143.
25 J. Zhuang, A. A. Bokov, N. Zhang, J. Zhang, J. Zhao, S. Yang, W. Ren and Z.-G. Ye, *Cryst. Growth Des.*, 2018, **18**, 4503-4510.
26 Z. Luo, N. Zhang, Z. Liu, J. Zhuang, J. Zhao, W. Ren and Z.-G. Ye, *J. Mater. Chem. C*, 2018, **6**, 9216-9223.
27 S. Zhang, D.-Y. Jeong, Q. Zhang and T. R. Shrout, *J. Cryst. Growth*, 2003, **247**, 131-136.
28 W. Bixia, W. Xiaoqing, R. Wei and Y. Zuo-Guang, *IEEE. T. Ultrason. Ferr.*, 2015, **62**, 1016-1021.
29 B. Wang, Y. Xie, J. Zhuang, X. Wu, W. Ren and Z.-G. Ye, *J. Appl. Phys.*, 2014, **115**, 084104.
30 R. A. Belan, H. N. Tailor, X. Long, A. A. Bokov and Z.-G. Ye, *J. Cryst. Growth*, 2011, **318**, 839-845.

31 Z. Liu, H. Wu, W. Ren and Z.-G. Ye, *Acta Mater.*, 2018, **149**, 132-141.

32 Y. M. Chiang, G. W. Farrey and A. N. Soukhojak, *Appl. Phys. Lett.*, 1998, **73**, 3683-3685.

33 C. Chen, H. Zhang, X. Zhao, H. Deng, L. Li, B. Ren, D. Lin, X. Li, H. Luo and Z. Chen, *J. Am. Ceram. Soc.*, 2014, **97**, 1861-1865.

34 D. E. Bugaris and H.-C. zur Loye, *Angew. Chem. Int. Edit.*, 2012, **51**, 3780-3811.

35 S. Zhang, L. Lebrun, S. Rhee, R. E. Eitel, C. A. Randall and T. R. Shrout, *J. Cryst. Growth*, 2002, **236**, 210-216.

36 S. Zhang, C. A. Randall and T. R. Shrout, *Jpn. J. Appl. Phys.*, 2004, **43**, 6199.

37 S. E. Park, S. J. Chung and I. T. Kim, *J. Am. Ceram. Soc.*, 1996, **79**, 1290-1296.

38 B. Noheda, D. Cox, G. Shirane, R. Guo, B. Jones and L. Cross, *Phys. Rev. B*, 2000, **63**, 014103.

39 Z. Luo, J. Zhuang, Z. Liu, N. Zhang, W. Ren and Z.-G. Ye, *CrystEngComm*, 2020, **22**, 4544-4551.

40 Z. Pan, X. Jiang, J. Chen, L. Hu, H. Yamamoto, L. Zhang, L. Fan, X. a. Fan, Y. Li, G. Li, Y. Ren, Z. Lin, M. Azuma and X. Xing, *Inorg. Chem. Front.*, 2018, **5**, 1277-1281.

41 C. Randall, R. Eitel, B. Jones, T. Shrout, D. I. Woodward and I. M. Reaney, *J. Appl. Phys.*, 2004, **95**, 3633-3639.

42 W.-M. Zhu, H.-Y. Guo and Z.-G. Ye, *Phys. Rev. B*, 2008, **78**, 014401.

43 E. E. Richard, A. R. Clive, R. S. Thomas, W. R. Paul, H. Wes and P. Seung-Eek, *Jpn. J. Appl. Phys.*, 2001, **40**, 5999.

44 Q. Zhang, Z. Li, F. Li, Z. Xu and X. Yao, *J. Am. Ceram. Soc.*, 2010, **93**, 3330-3334.

45 S. Zhang, F. Li, X. Jiang, J. Kim, J. Luo and X. Geng, *Prog. Mater. Sci.*, 2015, **68**, 1-66.

46 X. Liu, S. Zhang, J. Luo, T. R. Shrout and W. Cao, *J. Appl. Phys.*, 2009, **106**. 074112

47 H. Zhang, C. Chen, H. Deng, B. Ren, X. Zhao, D. Lin, X. Li and H. Luo, *J. Mater. Chem. C*, 2014, **2**, 10124-10128.

48 J. Íñiguez, D. Vanderbilt and L. Bellaiche, *Phys. Rev. B*, 2003, **67**, 224107.

49 J. Chen, K. Nittala, J. L. Jones, P. Hu and X. Xing, *Appl. Phys. Lett.*, 2010, **96**, 252908.

50 I. Grinberg and A. Rappe, *Phys. Rev. Lett.*, 2007, **98**, 037603.

51 I. Grinberg, M. Suchomel, W. Dmowski, S. Mason, H. Wu, P. Davies and A. Rappe, *Phys. Rev. Lett.*, 2007, **98**, 107601.

52 J. Chaigneau, J. Kiat, C. Malibert and C. Bogicevic, *Phys. Rev. B*, 2007, **76**, 094111.

53 B. Kim, P. Tong, D. Kwon, J. M. S. Park and B. G. Kim, *J. Appl. Phys.*, 2009, **105**, 114101.

54 L. Kong, G. Liu, S. Zhang and W. Yang, *Appl. Phys. Lett.*, 2015, **106**, 232901.

55 J. L. Jones, E. Aksel, G. Tutuncu, T.-M. Usher, J. Chen, X. Xing and A. J. Studer, *Phys. Rev. B*, 2012, **86**, 024104.

56 K. V. Lalitha, A. N. Fitch and R. Ranjan, *Phys. Rev. B*, 2013, **87**, 064106.

57 L. K. V, A. K. Kalyani and R. Ranjan, *Phys. Rev. B*, 2014, **90**, 224107.

58 K. Datta, S. Gorfman and P. A. Thomas, *Appl. Phys. Lett.*, 2009, **95**, 251901.

59 K. Datta, D. Walker and P. A. Thomas, *Phys. Rev. B*, 2010, **82**, 144108.

60 X. Lv, X.-x. Zhang and J. Wu, *J. Mater. Chem. A*, 2020, **8**, 10026-10073.

61 A. K. Tagantsev, L. E. Cross and J. Fousek, *Domains in ferroic crystals and thin films*, Springer, New York, 2010.

62 A. A. Bokov, X. Long and Z.-G. Ye, *Phys. Rev. B*, 2010, **81**, 172103.

63 Z.-G. Ye and M. Dong, *J. Appl. Phys.*, 2000, **87**, 2312-2319.

64 H. Y. Zhang, X. G. Chen, Y. Y. Tang, W. Q. Liao, F. F. Di, X. Mu, H. Peng and R. G. Xiong, *Chem. Soc. Rev.*, 2021, **50**, 8248-8278.

65 A. Gruverman, M. Alexe and D. Meier, *Nat. Commun.*, 2019, **10**, 1661.

66 B. Wang, Doctor of Philosophy, Simon Fraser University, 2016.

67 K. A. Schönau, L. A. Schmitt, M. Knapp, H. Fuess, R.-A. Eichel, H. Kungl and M. J. Hoffmann, *Phys. Rev. B*, 2007, **75**, 184117.

68 B. Noheda, *Curr. Opin. Solid State Mater. Sci.*, 2002, **6**, 27-34.

69 B. Noheda, D. E. Cox, G. Shirane, S. E. Park, L. E. Cross and Z. Zhong, *Phys. Rev. Lett.*, 2001, **86**, 3891-3894.

70 Z. Liu, Z. Luo, C. Wang, H. Wu, N. Zhang, H. Liu, W. Ren and Z.-G. Ye, *Ceram. Int.*, 2018, **44**, S189-S194.

71 A. R. Paterson, J. Zhao, Z. Liu, X. Wu, W. Ren and Z.-G. Ye, *J. Cryst. Growth*, 2018, **486**, 38-44.

72 Z. Tang, J. Zhuang, A. A. Bokov, Z. Luo, S. P. Kubrin, I. P. Raevski, M. Ma, N. Zhang, J. Zhang, Z. Liu, W. Ren and Z.-G. Ye, *Cryst. Growth Des.*, 2021, **21**, 3082-3092.

73 D. Zekria, A. Glazer, V. Shuvaeva, J. Dec and S. Miga, *J. Appl. Crystallogr.*, 2004, **37**, 551-554.

74 L. M. Eng and H. J. Güntherodt, *Ferroelectrics*, 2000, **236**, 35-46.

75 J. Hlinka and P. Márton, *Phys. Rev. B*, 2006, **74**, 104104.